Effect of Interplanetary Shocks on the *AL* and *Dst* Indices

M. L. Mays,[1] W. Horton,[1] J. Kozyra,[2] T. H. Zurbuchen,[2] C. Huang,[3] and E. Spencer[4]

Received 12 March 2007; revised 23 March 2007; accepted 1 May 2007; published 6 June 2007.

[1] The question of how much interplanetary shock (IP) events contribute to the geoeffectiveness of solar wind drivers is assessed through numerical experiments using the WINDMI model, a physics-based model of the solar wind-driven magnetosphere-ionosphere system. Analytic fits to solar wind input parameters ($B_{\perp}^{IMF}$, u_{sw}, n_{sw}) allowed shocks and associated shock-sheath plasma to be removed while leaving other features of the solar wind driver undisturbed. Percent changes in WINDMI-derived *AL* and *Dst* indices between runs with and without the observed shock and sheath signatures were taken as a measure of its relative contribution to the geoeffectiveness. The major magnetic storms during 15–24 April 2002 and 3–6 October 2000 were selected for this experiment. In both cases, the IP shock and sheath features contributed significantly to the geoeffectiveness of the solar wind driver. The magnetic field compressional jump is important to producing the changes in the *AL* during these two storm intervals.
Citation: Mays, M. L., W. Horton, J. Kozyra, T. H. Zurbuchen, C. Huang, and E. Spencer (2007), Effect of Interplanetary Shocks on the *AL* and *Dst* Indices, *Geophys. Res. Lett.*, *34*, L11104, doi:10.1029/2007GL029844.

1. Introduction

[2] Interplanetary coronal mass ejections (ICMEs) are the interplanetary counterparts of coronal mass ejections (CMEs) at the Sun and are observed as enhanced magnetic structures in the solar wind lasting on the order of a day [*Zurbuchen and Richardson*, 2006]. Magnetic clouds (MCs) are a subclass of ICMEs with above-average strength magnetic fields which rotate smoothly through a large angle in a low beta plasma. Earth-directed Halo ICMEs often trigger geomagnetic storms such as the storms of 3–6 October 2000 and 15–24 April 2002. Interplanetary (IP) shocks and their resulting geomagnetic activity are usually caused by Halo ICMEs and their associated dynamic interaction regions, also known as ''sheath regions'' [*Gosling et al.*, 1990]. These sheath regions are accelerated due to the momentum exchange from the fast CME, and they have enhanced densities and temperatures, since they have interacted with the shock. Solar wind velocity and magnetic field strength variation across interplanetary shocks are correlated with the *Dst* index [*Echer et al.*, 2004]. Shock effects on the aurora as measured by the FAST and DMSP satellites have been studied by *Zhou et al.* [2003]. It was found that there was a significant increase in electron precipitation the dawnside and duskside auroral oval zone after the shock/pressure pulse arrivals.

[3] In order to understand the effect of IP shock/sheath events on geomagnetic activity, we use the WINDMI model which uses the solar wind driving dynamo voltage $V_{sw}(t)$ derived from Advanced Composition Explorer (ACE) satellite data [*Stone et al.*, 1998] as input and outputs a predicted westward auroral electrojet index (*AL*) and disturbance storm time index (*Dst*). We construct analytic solar wind plasma fields from ACE data for the 3–6 October 2000 event and derive an analytic input driving voltage. There are three basic phenomena that can lead to perturbations in the *AL* and *Dst*: 1) the CME, as defined by its composition or magnetic field configuration 2) the sheath compressed solar wind and 3) the shock itself. The role of the shock events are examined by removing both the shock and sheath features individually from each analytic plasma field: solar wind density, velocity, and interplanetary magnetic field (IMF) magnitude, then examining the change in the WINDMI output of *AL* and *Dst*.

2. WINDMI Model and ACE Data Methodology

[4] We use the low dimensional WINDMI physics model of eight coupled ODE's which conserves energy and charge in the solar-wind driven magnetosphere-ionosphere system [*Horton and Doxas*, 1998]. WINDMI outputs a predicted *AL* and *Dst* index and with the solar wind driving and ionospheric damping, even at constant solar wind dynamo voltage there is a rich spectrum of possible magnetosphere-ionosphere states.

[5] Measurements of solar wind proton density, solar wind velocity and the IMF in GSM coordinates for the two geomagnetic storm periods are available from the ACE satellite. We use these quantities to derive the input dynamo driving voltage for the WINDMI model. The dynamo driving voltage $V_{sw}(t)$ was calculated from the analytic data using a formula given by *Siscoe et al.* [2002] and *Ober et al.* [2003] for the coupling of the solar wind to the magnetopause using the solar wind dynamic pressure P_{sw} to determine the standoff distance. The formula for V_{sw} is given by $V_{sw}(\mathrm{kV}) = 30.0(\mathrm{kV}) + 57.6E_{sw}(\mathrm{mV/m})P_{sw}^{-1/6}(\mathrm{nPa})$ where $E_{sw} = u_{sw}(B_y^2 + B_z^2)^{1/2}\sin(\frac{\theta}{2})$ is the solar wind electric field with respect to the magnetosphere and the dynamic solar wind pressure $P_{sw} = n_{sw}m_p u_{sw}^2$. Here m_p is the mass of a proton and only the proton density contribution has been included in n_{sw}, even though the He can provide important contributions to the dynamic pressure of the plasma. The IMF clock angle θ is given by $\tan^{-1}(B_y/B_z)$ and u_{sw} is the solar wind flow velocity.

[1]Institute for Fusion Studies, University of Texas at Austin, Austin, Texas, USA.
[2]Department of Atmospheric, Oceanic and Space Sciences, University of Michigan, Ann Arbor, Michigan, USA.
[3]MIT Haystack Observatory, Westford, Massachusetts, USA.
[4]Center for Space Engineering, Utah State University, Logan, Utah, USA.

0094-8276/07/2007GL029844

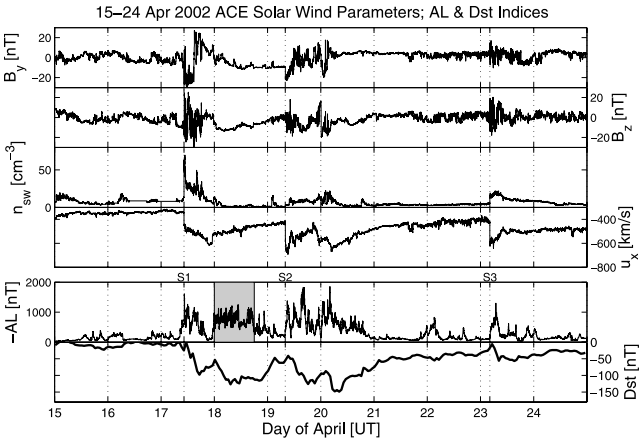

Figure 1. (top plots) ACE solar wind data for 15–24 April 2002 in GSM coordinates showing the interplanetary magnetic field components B_y and B_z, proton number density n_{sw}, and solar wind flow velocity $u_x(t)$. Three interplanetary shocks are identified by S1, S2, S3 occurring at 1020 UT 17 April, 0801 UT 19 April, and 0414 UT 23 April. (bottom plot) The corresponding time advanced *AL* and *Dst* data during this period shows substorm (shaded) and storm activity.

[6] The *AL* index is derived from measurements of the horizontal component of the Earth's magnetic field at stations located along the auroral oval in the Northern hemisphere [*Rostoker*, 1972]. The minimum values are taken to be the strongest activity of the westward auroral electrojet which is given by the region 1 field aligned current in the model, that closes in the nightside magnetosphere through the nightside auroral ionosphere. The *Dst* index is obtained from the measurement of the Earth's magnetic field from observatories that are sufficiently distant from the auroral and equatorial electrojets [*Sugiura*, 1964]. The *Dst* index is compared to the output from the WINDMI model through the ring current energy W_{rc} using the Dessler-Parker-Schopke relation [*Dessler and Parker*, 1959].

3. WINDMI Analysis

3.1. Period 15–24 April 2002

[7] In Figure 1 ACE data during this period shows three fast forward shock events which signal the arrival at Earth of CMEs from solar eruptions on 15, 17, and 21 April. ACE IMF data and compositional signatures (elevated oxygen charge states O^{7+}/O^{6+} and unusually high Fe charge states) were used to identify the signatures of the ICME in the data. The first shock event (S1) was observed by ACE at 1020 UT on 17 April moving at the calculated shock speed of 480 km/s and is associated with a halo CME with brightness asymmetry observed by SOHO/LASCO at 0350 UT on 15 April moving at the plane-of-sky speed of 720 km/s away from the Sun [*Manoharan et al.*, 2004]. The CME driving the shock is observed by ACE as a MC beginning at the start of 18 April and continuing until approximately 1900 UT. The shock and sheath features in the data are taken from 1020 UT (S1) to 1450 UT on 17 April. Seven sawtooth oscillations were observed on 18 April from about 0200 UT to 2100 UT whose signature can be seen in the *AL* shown in the bottom panels of Figure 1 as the shaded region. The *Dst*, also shown in this figure, reaches a −127 nT during this time.

[8] The second shock event (S2) was observed at 0801 UT on 19 April with a speed of 650 km/s and is associated with a halo CME with outline asymmetry which left the Sun at 0826 on 17 April moving with the plane-of-sky speed of 1240 km/s [*Cane and Richardson*, 2003]. The shock on April 19 was followed by a more complicated solar wind disturbance observed by ACE from 1500–2000 UT 19 April and 1000 UT 20 April to 1200 UT 21 April likely resulting from a subsequent CME which dynamically interacts with the perturbation ahead. The interacting signatures looked qualitatively comparable to the well-documented case of October–November 2003 [*Zurbuchen et al.*, 2004], but with clear signatures of solar wind between the two interacting CMEs. The shock/sheath features are taken from 0801 UT (S2) to 1300 UT on 19 April. This solar wind disturbance triggered a magnetic storm with *Dst* minima of −126 nT and −124 nT building up in the main phase and −148 nT and −149 nT at storm peak. The third shock event (S3) arrived during the recovery phase at 0413 UT on 23 April with a speed of 680 km/s and is associated with an X-class flare and partial halo CME with outline asymmetry leaving the Sun at 0127 UT on 21 April with the plane-of-sky speed of 2393 km/s. The magnetosphere was clipped by the shock/sheath region rather than the ICME, producing a weak magnetic storm with minimum *Dst* of only −56 nT. Halo CMEs experience maximum projection effects in coronagraph images and therefore the plane-of-sky speeds should be taken as a lower limit of the actual speed. The shock dates and times are listed in Table 1 and the date, time and speed of the associated CMEs are taken from the SOHO LASCO CME catalog [*Yashiro et al.*, 2004].

[9] Analysis of the WINDMI *AL* and *Dst* results using ACE data as input is given by *Spencer et al.* [2007]. Here we compare these results to WINDMI output driven by analytic fits to the same solar wind data. The analytic fits to

Table 1. A Listing of Observed ACE IP Shock Dates, Times, and Calculated Speeds (Assuming a Parallel Shock) During 15–24 April 2002, With Associated SOHO CME Times and Speeds[a]

Shock, UT	Speed, km/s	ICME Signature	CME, UT	Speed, km/s
April 17 1020	480	1800 UT 17 April-1900 UT 18 April	April 15 0350	720
April 19 0801	650	1500–2000 UT 19 April 1000 UT 20 April-1200 UT 21 April	April 17 0826	1240
April 23 0414	680	none	April 21 0127	2393

[a]Dates of observed magnetic cloud structure in ACE IMF B_y, B_z, and clock angle are also listed.

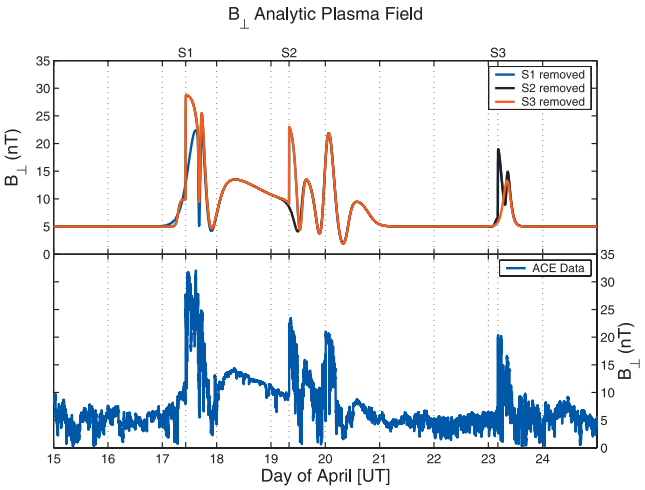

Figure 2. (bottom) ACE data for the solar wind $B_\perp = (B_y^2 + B_z^2)^{1/2}$ during the April 2002 storm. (top) Analytic parameter for the solar wind $B_\perp$ for which certain shock/sheath features have been removed from the analytic shock field based on the ACE data.

the ACE data were constructed using hyperbolic tangent functions. To study the role of the shock, the shock and sheath features are removed from the solar wind parameters (u_{sw}, n_{sw}, $B_\perp$) individually while the ICME signature is kept. The shock and sheath features were removed from the data for the duration of the shock time up until before the associated ICME signatures. The methodology is to test the effect of each shock/sheath feature on the geospace response by removing the feature from the analytic fields while the other fields downstream remain unchanged.

[10] Figure 2 shows how the model fields without the compressional jumps in the solar wind $B_\perp = (B_y^2 + B_z^2)^{1/2}$ are expressed for the April 2002 storm. The three curves in the top panel give the analytic model $B_\perp$ profile with the first S1 (dashed line), second S2 (dotted line), and third S3 (solid line) shock/sheath features individually removed. The bottom panel shows the ACE magnetometer data for the $B_\perp$ signal.

[11] The solar wind driving voltage was calculated using the equation given in Section 2 with our analytic solar wind fields with and without the shock/sheath feature. Using this input solar wind driving voltage the model outputs were compared with and without the shock/sheath. In Figure 3 we compare WINDMI results from runs using both data and analytic input fields from which the shock/sheath feature has been removed from $B_\perp$. The analytic shock field $B_\perp$ without all three $\delta B_\perp$ shock/sheath features (top panel of Figure 2), and ACE data for the u_{sw} and n_{sw} parameters were used to derive the input solar wind dynamo voltage shown in the top panel of Figure 3 (solid black line). WINDMI *−AL* and *Dst* results for this input are shown in the middle and bottom panels (dashed lines), respectively. When the $\delta B_\perp$ shock/sheath feature is removed there is a significant decrease of 50% in the *AL* peaks −1600 nT (17 April 1100 UT), −1824 nT and −1851 nT (19 April 1648 UT and 20 April 0451 UT), and −1297 nT (23 April 0741 UT) associated with these shocks. Model results for the *Dst* (bottom panel of Figure 3) show a *−Dst* decrease of 10−20% for roughly 12 hours after the first shock (17 April 1120 UT to 18 April 0700 UT) and a decrease of 20%−30% after the second shock (19 April 0900 UT to 20 April 0400 UT).

[12] The jump $\delta B_\perp$ has the most significant impact on the *AL* and *Dst* compared to the other parameters. Removing the shock/sheath features from u_{sw} produces a slight decrease of 15%, 25% and 10% in the first, second, and third *AL* peaks respectively. There is only a slight increase of 10% and 5% of the first and third *AL* peaks when the shock/sheath features are removed from n_{sw}. The compressional jump δn_{sw} is only ~2 cm^{-3} for the second shock event. When the shock/sheath features are removed from all of the plasma fields ($B_\perp^{IMF}$, u_{sw}, n_{sw}) the *−AL* peaks decrease by a similar amount as when the $\delta B_\perp$ features are removed only. The jump $\delta B_\perp$ has the most impact on producing the three *−AL* peaks during this storm. The second shock/sheath combination on 19 April at 0801 UT which produced *AL* peaks of −1824 nT and −1851 nT is the most effective of the three shocks.

3.2. Period 3−6 October 2000

[13] An unusual feature of the 3−6 October 2000 solar wind driver was the appearance of a fast forward shock advancing into a preceding magnetic cloud [*Wang et al.*, 2003]. ACE data shows a magnetic cloud from 3 October at 1018 UT through 5 October at 0534 UT lasting about 42 hours. The signature of the magnetic cloud can be seen from the sinusoid-like waveforms of B_y^{IMF} and B_z^{IMF} as the IMF clock angle changes linearly through an angle of 180° during this period. The fast forward shock occurs at 0240 UT on 5 October with a calculated shock speed of 534 km/s and compression ratio of 2.3. There are jumps in the velocity from 364 km/s to 460 km/s, in the proton

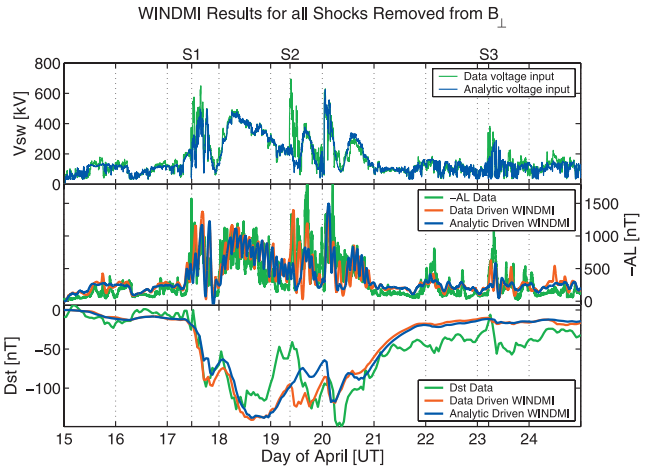

Figure 3. WINDMI results for V_{sw} input derived from solar wind parameter data or analytic parameters for which all three shock/sheath features have been removed from $B_\perp$. (top) Analytic shock field $B_\perp$ without the shock/sheath features (Figure 2, top plot), and ACE data for the u_{sw} and n_{sw} parameters was used to derive the input solar wind dynamo voltage. WINDMI (middle) *−AL* and (bottom) *Dst* results for this input (dashed lines).

density from 7 cm^{-3} to 16 cm^{-3}, and in perpendicular magnetic field from 7 nT to 16 nT across the shock front.

[14] The *AL* data shows a first large spike with a peak of −1938 nT occurring at 0651 UT on 5 October 2000. A second, larger spike of approximately −2790 nT in the *AL* index occurs at 1210 UT on 5 October 2000 initiated by a strong southward IMF excursion detected at ACE about an hour earlier. Periodic substorms occur in the interval of 0600–1200 UT 4 October and have been identified as sawtooth oscillations by *Huang et al.* [2003] and *Reeves et al.* [2003]. The *Dst* minimum of −180 nT is reached on 5 October slightly after the strong southward IMF surge. Consistent with April 2002 analysis, when the shock/sheath feature is removed from $B_\perp$ the first *AL* peak of −1938 nT occurring at 0720 UT 5 October 2000 decreased by ∼50%. There is also a decrease of $-Dst$ by ∼25% after the shock arrival time. The *AL* peak only decreases by 10% when the shock/sheath is removed from u_{sw} and the removal of the feature from n_{sw} produces an increase of 10% in the *AL* peak. Again, when the shock is dropped from all three plasma fields the result is similar to removing the $\delta B_\perp$ shock only. These results demonstrate that the first large *AL* peak was triggered by the shock/sheath front, and most strongly by the $\delta B_\perp$ jump.

4. Summary

[15] The question of how much IP shock/sheath events contribute to the geoeffectiveness of solar wind drivers was examined based on a series of numerical experiments with WINDMI using observed solar wind drivers for the 15–24 April 2002 and 3–6 October 2000 events, each of which had interesting shock features. In these experiments, analytic fits to solar wind input parameters ($B_\perp^{IMF}$, u_{sw}, and n_{sw}) allowed shock/sheath features to be easily removed while leaving other features of the solar wind driver undisturbed. Percent changes in WINDMI-derived *AL* and *Dst* indices between runs with and without the observed shock/sheath feature were taken as a measure of its relative contribution to the geoeffectiveness. The main results of this study are the following:

[16] 1. The interplanetary shock/sheath events during these storm periods are strongly related to storm and substorm geomagnetic activity predicted by the WINDMI model.

[17] 2. The $\delta B_\perp$ jumps at the shocks/sheath have a strong impact on the three *AL* peaks during the April 2002 storm. During the October 2000 storm the first large *AL* spike was triggered by the shock/sheath feature in $B_\perp$. The *Siscoe et al.* [2002] solar wind dynamo voltage includes contributions from the number density, clock angle, and B_y^{IMF} ($B_\perp^{IMF} = (B_y^2 + B_z^2)^{1/2}$) which are not included in the rectified $u_{sw}\ B_z\ L_y$ dynamo voltage more typically used. This is particularly important for the April 2002 shocks in which, for example, the second shock had a $\delta B_z^{IMF} < 1$ nT while $\delta B_y^{IMF} \sim 10$ nT therefore producing dynamo voltage $V_{sw} = 600$ kV while the rectified voltage is only 200 kV.

[18] The solar wind-magnetosphere coupling dynamics is most sensitive to variations in the solar wind velocity and interplanetary magnetic field. This can be seen from the equation for the input Siscoe solar wind dynamo voltage where the input $V_{sw} \propto u_{sw}^{2/3}\ n_{sw}^{-1/6}\ B_\perp^{1/2}$ so it is expected that the removal of the shock compressional feature in the velocity and magnetic field parameters to decrease the driving voltage V_{sw}, and in the number density to increase V_{sw}. During these storms the magnetic field components have a 1.5–3 times increase across the shock front while the velocity does not increase by more than 1.5 times. The jump in the number density can be as high as 4 times the upstream value, however, the $n_{sw}^{-1/6}$ dependence in the calculated V_{sw} hides this effect. Also shock features in the velocity and number density increase the solar wind dynamic pressure which causes the magnetopause to move close to the Earth and produces stronger coupling.

[19] **Acknowledgments.** This work was partially supported by NSF grants ATM-0539099, ATM-0402163, and NASA grant NNG05GJ89G. The solar wind plasma and magnetic field data were obtained from ACE at NASA's CDAWeb site. The SOHO LASCO CME Catalog is generated and maintained by NASA and The Catholic University of America in cooperation with the Naval Research Laboratory (http://cdaw.gsfc.nasa.gov/CME_list/). The geomagnetic indices used were obtained from the World Data Center for Geomagnetism in Kyoto, Japan.

References

Cane, H. V., and I. G. Richardson (2003), Interplanetary coronal mass ejections in the near-Earth solar wind during 1996–2002, *J. Geophys. Res.*, *108*(A4), 1156, doi:10.1029/2002JA009817.

Dessler, A., and E. N. Parker (1959), Hydromagnetic theory of geomagnetic storms, *J. Geophys. Res.*, *64*, 2239–2259.

Echer, E., M. V. Alves, and W. D. Gonzalez (2004), Geoeffectiveness of interplanetary shocks during solar minimum (1995–1996) and solar maximum (2000), *Sol. Phys.*, *221*, 361–380, doi:10.1023/B:SOLA.0000035045.65224.f3.

Gosling, J. T., S. J. Bame, D. J. McComas, and J. L. Phillips (1990), Coronal mass ejections and large geomagnetic storms, *Geophys. Res. Lett.*, *17*, 901–904.

Horton, W., and I. Doxas (1998), A low-dimensional dynamical model for the solar wind driven geotail-ionosphere system, *J. Geophys. Res.*, *103*(A3), 4561–4572.

Huang, C.-S., J. Foster, G. Reeves, G. Le, H. Frey, C. Pollock, and J.-M. Jahn (2003), Periodic magnetospheric substorms: Multiple space-based and ground-based observations, *J. Geophys. Res.*, *108*(A11), 1411, doi:10.1029/2003JA009992.

Manoharan, P. K., N. Gopalswamy, S. Yashiro, A. Lara, G. Michalek, and R. A. Howard (2004), Influence of coronal mass ejection interaction on propagation of interplanetary shocks, *J. Geophys. Res.*, *109*, A06109, doi:10.1029/2003JA010300.

Ober, D. M., N. C. Maynard, and W. J. Burke (2003), Testing the Hill model of transpolar potential saturation, *J. Geophys. Res.*, *108*(A12), 1467, doi:10.1029/2003JA010154.

Reeves, G., et al (2003), Image, polar, and geosynchronous observations of substorm and ring current ion injection, in *Disturbances in Geospace: The Storm-Substorm Relationship*, *Geophys. Monogr. Ser.*, vol. 142, edited by A. S. Sharma, Y. Kamide, and G. S. Lakhina, pp. 91–101, AGU, Washington, D. C.

Rostoker, G. (1972), Geomagnetic indices, *Rev. Geophys.*, *10*, 935.

Siscoe, G. L., N. U. Crooker, and K. D. Siebert (2002), Transpolar potential saturation: Roles of region-1 current system and solar wind ram pressure, *J. Geophys. Res.*, *107*(A10), 1321, doi:10.1029/2001JA009176.

Spencer, E., W. Horton, M. L. Mays, I. Doxas, and J. Kozyra (2007), Analysis of the October 3–7 2000 and April 15–24 2002 geomagnetic storms with an optimized nonlinear dynamical model, *J. Geophys. Res.*, *112*, A04590, doi:10.1029/2006JA012019.

Stone, E. C., A. M. Frandsen, R. A. Mewaldt, E. R. Christian, D. Margolies, J. F. Ormes, and F. Snow (1998), The Advanced Composition Explorer, *Space Sci. Rev.*, *86*, 1–22, doi:10.1023/A:1005082526237.

Sugiura, M. (1964), Hourly values of equatorial Dst for the IGY, *Ann. Int. Geophys. Year*, *35*(9), 945.

Wang, Y., P. Ye, S. Wang, and X. Xue (2003), An interplanetary cause of large geomagnetic storms: Fast forward shock overtaking preceding magnetic cloud, *Geophys. Res. Lett.*, *30*(13), 1700, doi:10.1029/2002GL016861.

Yashiro, S., N. Gopalswamy, G. Michalek, O. C. St. Cyr, S. P. Plunkett, N. B. Rich, and R. A. Howard (2004), A catalog of white light coronal mass ejections observed by the SOHO spacecraft, *J. Geophys. Res.*, *109*, A07105, doi:10.1029/2003JA010282.

Zhou, X.-Y., R. J. Strangeway, P. C. Anderson, D. G. Sibeck, B. T. Tsurutani, G. Haerendel, H. U. Frey, and J. K. Arballo (2003), Shock aurora: FAST and DMSP observations, *J. Geophys. Res.*, *108*(A4), 8019, doi:10.1029/2002JA009701.

Zurbuchen, T. H., and I. G. Richardson (2006), In-situ solar wind and magnetic field signatures of interplanetary coronal mass ejections, *Space Sci. Rev.*, *123*, 31–43, doi:10.1007/s11214-006-9010-4.

Zurbuchen, T. H., G. Gloeckler, F. Ipavich, J. Raines, C. W. Smith, and L. A. Fisk (2004), On the fast coronal mass ejections in October/November 2003: ACE-SWICS results, *Geophys. Res. Lett.*, *31*, L11805, doi:10.1029/2004GL019461.

W. Horton and M. L. Mays, Institute for Fusion Studies, University of Texas at Austin, RLM 11.222, 1 University Station C1500, Austin, TX 78712-0262, USA. (lmays@physics.utexas.edu)

C. Huang, MIT Haystack Observatory, Westford, MA 01886, USA.

J. Kozyra and T. H. Zurbuchen, Department of Atmospheric, Oceanic and Space Sciences, University of Michigan, Ann Arbor, MI 48109, USA.

E. Spencer, Center for Space Engineering, Utah State University, Logan UT 84322, USA.